PHYSICAL REVIEW B **73**, 060201(R) (2006)

Intermediate-range order in molten network-forming systems

Bevan K. Sharma and Mark Wilson
Department of Chemistry, University College London, 20 Gordon Street, London WC1H 0AJ, United Kingdom
(Received 6 January 2006; published 16 February 2006)

The structural origin of intermediate-range order in two archetypal network-forming liquids, $GeSe_2$ and $ZnCl_2$, is investigated via molecular dynamics computer simulation. Relatively simple ionic models, in which a proper description of ion polarization effectively controls the network connectivity, are shown to be capable of showing a first-sharp diffraction peak in the Bhatia-Thornton concentration-concentration structure factor. This feature is shown to arise from the presence of percolating edge-sharing polyhedral units which act to disrupt a corner-sharing network and introduce addition cation density fluctuations on both short- and intermediate-range length scales.

DOI: 10.1103/PhysRevB.73.060201 PACS number(s): 61.20.Ja, 61.25.−f

Many network-forming amorphous systems display a first-sharp diffraction peak (FSDP) in the total structure factor, indicative of the presence of intermediate-ranged order (IRO), that is, structural ordering beyond that imposed by (short-range) atom packing arrangements.[1,2] The structural origins of this order remains a topic of debate with theories based on underlying crystalline order[3] and the presence of an ordered void network[4,5] both advanced. In addition, simulation studies indicate that this length scale dominates the system dynamics around the glass transition temperature[6] with potential ramifications for glass-formation theories.[7] In the MX_2 stoichiometry, $GeSe_2$ and $ZnCl_2$ represent an archetypal pair of materials having IRO with a network structure which can be considered as constructed from a mix of corner-sharing and edge-sharing MX_4 tetrahedra (M=metal cation, X=anion). Both systems show a FSDP at scattering angles corresponding to $k_{FSDP} \sim 1$ Å^{-1} (compared with the principal peak at $k_{PP} \sim 2$ Å^{-1}) in their structure factors.[8–10] Furthermore, the existence of suitable isotopes allows the partial structure factors to be experimentally resolved for both systems[8,10,11] rendering these systems excellent targets for simulation models. Neutron scattering studies[8,10] indicate that the respective FSDPs are dominated by the cation sublattice (although this view has been questioned[12]). Both systems display complex morphology changes (on both short and intermediate length scales) as a function of temperature[10,13] and pressure.[14,15] Despite their clear similarities, these systems also show distinct differences often assigned to a fundamental difference in their inherent bonding. $GeSe_2$, for example, shows a small fraction of homopolar bonds[16,17] not present in $ZnCl_2$, which may have implications for network-dependent properties.

The difference in structure is naturally expressed in the Bhatia-Thornton structure factors, which separate structural (network) ordering from that imposed by the underlying chemistry (chemical ordering),[18,19] with $GeSe_2$ showing a significantly stronger FSDP in the concentration-concentration function $S_{CC}(k)$, indicative of chemical ordering on an intermediate length scale. Simulation work has tended to focus on the individual systems. For $GeSe_2$, *ab initio* electronic structure calculations have reproduced a large number of static and dynamic properties.[16,17] However, the emergence of a FSDP in $S_{CC}(k)$ is found to be heavily dependent upon the details of the calculation. Furthermore, pair-potential based models augmented with explicit three-body terms, which constrain specific bond angles, fail to reproduce such a feature.[20] An understanding of the structural origin of this FSDP in $S_{CC}(k)$ is, however, lacking. Massobrio *et al.*[16] define three classes of IRO in which structural disorder is correlated with the FSDP intensity. Class I encompasses near-perfect networks and have no FSDP in $S_{CC}(k)$. In class II, significant structural disorder leads to an FSDP, while in class III the degree of this disorder is such as to remove the FSDP.

In this Rapid Communication "simple" potential energy models are applied (using molecular dynamics) in order to focus on the factors controlling the IRO in these two systems. The simulation models are based on pair potentials in which the ions interact through their formal (valence) charges and through short-range repulsive functions, modeled as a Born-Mayer potential. In addition to the standard Born-Mayer potential parameters (a,B,C), which control the short-range and dispersion interactions, a description of the (many-body) polarization effects [the polarizable-ion model[21] (PIM)] is incorporated requiring an additional three parameters; α (the ion polarizability) and $\{b,c\}$ (the short-range damping parameters[22]). Full details of these models are given in Refs. 21 and 22. Potential parameter sets (Table I) are derived so as to reproduce a range of structural properties with the polarization terms restricted to the anions.[23] The polarization effects in network-forming systems effectively act to control the bond angles for the polyhedral linkages (the M-X-M bond angles). Dipoles induced on the bridging anions act to introduce negative charge in between two neighboring cations and, as a result, screen the cation-cation repulsive coulombic interaction[21] and hence narrow the M-X-M bond angle. In extreme cases (small cations and/or highly polarizable anions) this effect can be so great as to stabilize edge-sharing units in which a cation pair shares two anion bridges.[24] For systems such as $ZnCl_2$ and $GeSe_2$ the polarization effects are balanced such that the systems can be considered as a dynamic mix of corner-sharing and edge-sharing units. The relative flexibility of the PIM lies in the ability to readily stabilize both corner-sharing and edge-sharing polyhedral links as a function of the anion environment, rather than relying on more restrictive explicit bond-angle constraints.

Figure 1(a) shows the partial Faber-Ziman (FZ) structure

TABLE I. Potential parameters used in the present work. The ion-ion interactions are modeled using a Born-Mayer potential in which the short-range interaction is given by $U(r_{ij}) = B_{ij}\exp(-a_{ij}r_{ij}) - C_{ij}^6/r_{ij}^6$. The damping parameters, b and c, and dipole polarizability, α, are required for the polarizable-ion model.

ij	B_{ij} (a.u.)	a_{ij} (a.u.)	C_{ij}^6 (a.u.)
GeSe	199.34	1.556	380
SeSe	98.56	1.556	1001
ZnCl	43.72	1.600	44
ClCl	87.00	1.556	183
i	α_i (a.u.)	b (a.u.)	c (a.u.)
Se^{2-}	50.0	1.65	2.20
Cl^-	20.0	1.65	1.40

factors[25] for the $ZnCl_2$ and $GeSe_2$ models calculated at $T = 800$ K and 2400 K, respectively (in the liquid regimes for both systems) and at zero pressure. The strongest FSDPs are observed in the respective metal-metal functions, with significant features in the corresponding metal-anion functions. The major difference between these systems lies in the relative intensities of the FSDP in $S_{MM}(k_{FSDP})$ compared with the principal peak $[S_{MM}(k_{PP})]$. The feature in $GeSe_2$ is significantly more intense than in $ZnCl_2$ (~90% and ~55% of the principal peak heights, respectively) consistent with experiment[8,10,11] and *ab initio* simulation.[16]

The Bhatia-Thornton (BT) partial structure factors $[S_{CC}(k)$, $S_{NN}(k)$, and $S_{NC}(k)]$ may be expressed in terms of the Faber-Ziman functions as

$$S_{CC}(k) = c_M c_X\{1 + c_M c_X[[S_{MM}(k) - S_{MX}(k)] + [S_{XX}(k) - S_{MX}(k)]]\},$$

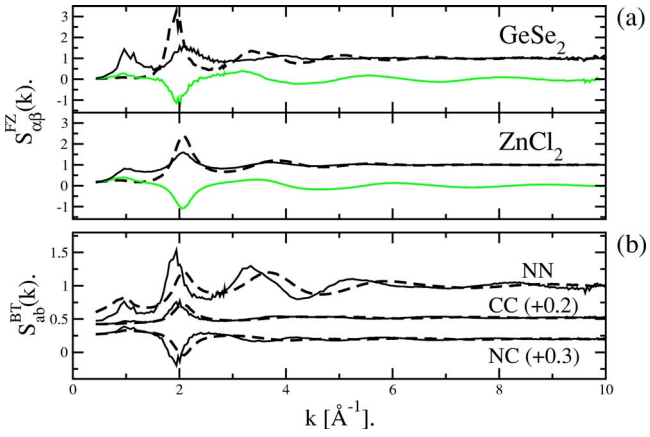

FIG. 1. (Color online) Partial structure factors for the $GeSe_2$ and $ZnCl_2$ models obtained at 800 and 2400 K, respectively. (a) Faber-Ziman functions. Key: solid dark line, metal-metal; solid light line, metal-anion; dashed line, anion-anion. (b) Bhatia-Thornton functions. Key: solid lines, $GeSe_2$; dashed lines, $ZnCl_2$. The $S_{CC}(k)$ and $S_{NC}(k)$ functions have been shifted along the y axis as indicated for clarity.

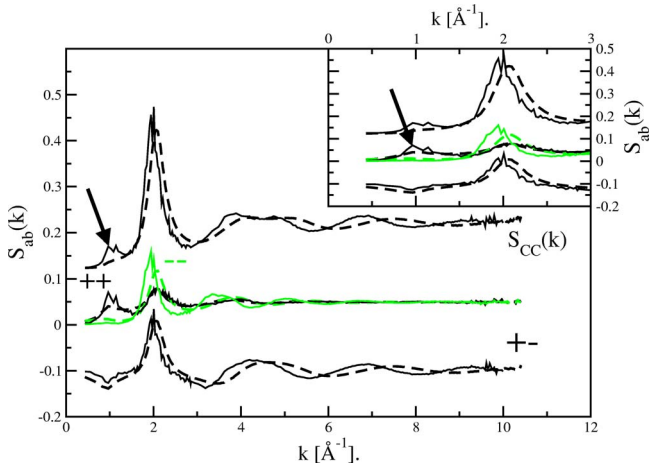

FIG. 2. (Color online) Breakdown of the Bhatia-Thornton concentration-concentration structure factors, $S_{CC}(k)$, into (weighted) Faber-Ziman functions for then $GeSe_2$ (solid lines) and $ZnCl_2$ (dashed lines) models. The $GeSe_2$ model shows a clear FSDP (indicated by an arrow) which is absent for $ZnCl_2$. The inset shows the low-k functions in order to emphasize the dominant role of $S_{MM}(k)$ (highlighted with an arrow) in forming the FSDP in $S_{CC}(k)$.

$$S_{NN}(k) = c_M^2 S_{MM}(k) + c_X^2 S_{XX}(k) + 2c_M c_X S_{MX}(k),$$

$$S_{NC}(k) = c_M c_X\{c_M[S_{MM}(k) - S_{MX}(k)] - c_X[S_{XX}(k) - S_{MX}(k)]\}. \quad (1)$$

Figure 1(b) shows the BT structure factors for the simulated $GeSe_2$ and $ZnCl_2$ systems. Clear FSDPs are observed in both $S_{NN}(k)$ functions (again, consistent with experiment[10]). Significantly, an FSDP appears in $S_{CC}(k)$ for the $GeSe_2$ model, but not for the $ZnCl_2$. Although recent scattering experiments suggest the appearance of an FSDP in $S_{CC}(k)$ in both systems,[11] the signature for $ZnCl_2$ appears significantly weaker than for $GeSe_2$. As a result, we envisage the two models considered here may represent extrema in terms of their IRO and its relation to $S_{CC}(k)$. Figure 2 shows the breakdown of $S_{CC}(k)$ into the weighted contributions from the FZ functions [Eq. (1)]. At $k \geqslant k_{PP}$ $S_{CC}(k)$ is a simple superposition of the three FZ functions, with the two like-like functions $[S_{MM}(k)$ and $S_{XX}(k)]$ equally weighted and $S_{MX}(k)$ weighted double [Eq. (1)]. At $k \leqslant k_{PP}$, however, $S_{XX}(k_{FSDP}) \sim 0$ and so $S_{CC}(k)$ approximates to a simple combination of $S_{MM}(k)$ and $S_{MX}(k)$ $[S_{CC}(k) \simeq c_M c_X\{1 + c_M c_X[S_{MM}(k) - 2S_{MX}(k)]\}]$. For the $ZnCl_2$ model these two functions effectively cancel out on the length scale associated with the FSDP. It appears, therefore, that the greater intensity of $S_{GeGe}(k)$ [compared with $S_{ZnZn}(k)$ in $ZnCl_2$] leads to an incomplete cancellation from the respective anion-cation function and hence to the significant FSDP in $S_{CC}(k)$.

In order to understand the structural origins of this difference in $S_{CC}(k_{FSDP})$, $S_{MM}(k)$ and $S_{MX}(k)$ are decomposed into additional partial structure factors generated by "coloring" each cation in terms of the local environment. A cation at the center of a tetrahedron which only corner shares with neighboring polyhedra is labeled "0," while those structural units

TABLE II. Percentage of cation-centered units colored according to their network connectivity.

	$GeSe_2$	$ZnCl_2$
0	17	45
1	57	36
2	26	19

containing one and two edge-sharing units are labeled "1" and "2," respectively.[16] Table II lists the fractions of each cation type for the two systems averaged over ~500 ps of molecular dynamics. The $GeSe_2$ model contains a significantly greater proportion of edge-sharing units. An additional six *MM* and three *MX* structure factors can be defined as

$$S^{ab}_{MM}(k) = \langle A^{a^*}_M(k) \cdot A^b_M(k) \rangle, \quad S^{aX}_{MX}(k) = \langle A^{a^*}_M(k) \cdot A_X(k) \rangle, \qquad (2)$$

where $\{a,b\}=\{0,1,2\}$.[26] Figure 3 shows the breakdown of the respective $S_{MM}(k)$ and $S_{MX}(k)$ structure factors into the (weighted) partial functions defined above. For $GeSe_2$, the strongest contributions to the FSDP in $S_{MM}(k)$ arise from $S^{11}_{MM}(k)$, $S^{12}_{MM}(k)$, and $S^{02}_{MM}(k)$, with $S^{12}_{MM}(k)$ and $S^{02}_{MM}(k)$ both having an FSDP intensity greater than that of the principal peak $[S_{MM}(k_{FSDP})/S_{MM}(k_{PP})=1.13$ and 1.79, respectively]. For $ZnCl_2$ the six functions appear similar in terms of the $S_{MM}(k_{FSDP})/S_{MM}(k_{PP})$ ratio (in the range 0.6 to 0.9), with each appearing to contribute significantly to the FSDP in $S_{ZnZn}(k)$ with their relative contributions dictated by the concentration weightings in Ref. 26. In addition, the $GeSe_2$ function FSDPs differ in position, with $k_{FSDP}=0.97$, 1.08, 1.02, and 1.03 Å^{-1} for $S^{01}_{MM}(k)$, $S^{02}_{MM}(k)$, $S^{11}_{MM}(k)$, and $S^{12}_{MM}(k)$, respectively. These differences indicate that the presence of a significant proportion of edge-sharing units in the $GeSe_2$ model exerts a major influence on the static structure by effectively breaking up the corner-sharing network and introducing subtle variations in the IRO. Further clues as to the nature of this network disruption are afforded by considering

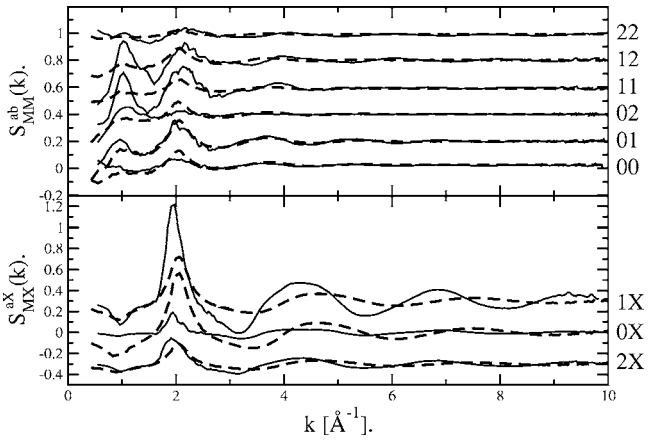

FIG. 3. Breakdown of the metal-metal (upper panel) and metal-anion (lower panel) Faber-Ziman structure factors in terms of cation environment. The functions are weighted by the respective concentrations of the colored cations.

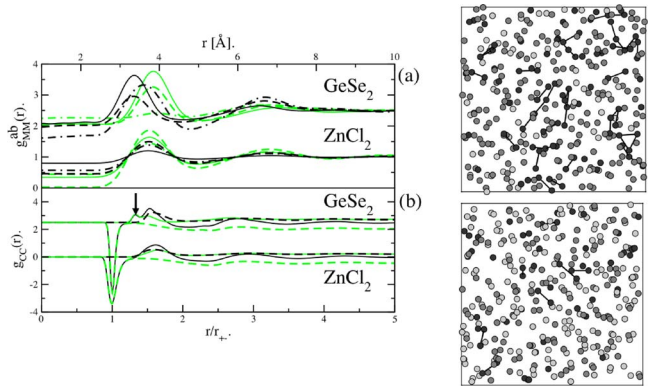

FIG. 4. (Color online) (a) Fourier transforms of the metal-metal functions shown in Fig. 3. (b) Real space Bhatia-Thornton concentration-concentration pair distribution function for the two systems along with the three Faber-Ziman contributions. The arrow highlights the extra feature apparent for $GeSe_2$ resulting from the presence of chains of edge-sharing tetrahedra. Key: solid dark line, $g_{CC}(r)$; solid light line, metal-metal; light dashed line, metal-anion; dark dashed line, anion-anion. (Right panel) Molecular graphics snapshots showing cations only for (top) $GeSe_2$ and (bottom) $ZnCl_2$. Key: dark circles, labeled 2; medium circles, labeled 1; light circles, labeled 0. Cations labeled 2 are joined by bonds to highlight the formation of significant chain structure in the $GeSe_2$ model.

the widths of the FSDPs in Fig. 3. The $S^{11}_{MM}(k)$, $S^{12}_{MM}(k)$, and $S^{02}_{MM}(k)$ functions show widths (at half the peak height) of 0.35, 0.39, and 0.67 Å^{-1}, respectively. The significantly greater width of $S^{02}_{MM}(k)$ at k_{FSDP} results from the pseudo-one-dimensional nature of the percolating edge-sharing chains. These chains are effectively charge neutral and so are only weakly bound to the network perpendicular to the chain major axis. This weak bonding results in the formation of an ordered intermediate-ranged length scale in addition to that imposed by the corner-sharing network. Unlike $S_{MM}(k)$, the $S_{MX}(k)$ functions appear to effectively map onto each other when the concentration weightings are accounted for. The difference in the two systems, therefore, lies in the relative intensities of $S_{MM}(k)$ which is directly correlated to the differing proportions of edge-sharing units.

Two further differences between the *MM* functions are noteworthy. First, both $S^{00}_{GeGe}(k)$ and $S^{22}_{GeGe}(k)$ are increasing as $k \to 0$ indicative of an effective "phase separation" or clustering of these colored cation sites. Secondly, the long-k oscillations appear quite different in the two sets of functions. For the $ZnCl_2$ model the six functions appear to contain oscillations (at $k \geqslant k_{PP}$) at approximately the same frequency. In the $GeSe_2$ model, however, both the oscillation frequencies and their intensities appear to differ significantly between the six functions. To further understand these differences the six functions defined in Eq. (2) are Fourier transformed to produce the corresponding real space partial pair distribution functions (pdfs), $g^{ab}_{MM}(r)$. Figure 4 (upper panel) shows the six partial pdfs for the two systems. As predicted from the high-k oscillations displayed by the functions in Fig. 3, the $ZnCl_2$ functions exhibit a single peak at ~3.75 Å. The $GeSe_2$ functions, however, display peaks on three length scales; $g^{00}_{GeGe}(r)$ and $g^{01}_{GeGe}(r)$ show a peak at ~3.86 Å,

$g^{11}_{GeGe}(r)$ at ~3.60 Å, and $g^{12}_{GeGe}(r)$ and $g^{22}_{GeGe}(r)$ at ~3.35 Å. The resolution of the different cation length scales supports the existence of relatively long-lived species built around corner-sharing and edge-sharing in the molten state. Figure 4 shows two molecular graphics snapshots of the respective cation distributions with the different polyhedral linkages highlighted. For the $GeSe_2$ system a significant number of the edge-sharing units form into chains. This percolation of the edge-sharing units leads to an effective clustering of these units with the resulting phase separation between the sites labeled 0 and 2 (as detected in the structure factors in Fig. 3). The presence of a cation labeled 2 precludes nearest-neighbors labeled 0 (since these neighbors must have at least one edge-sharing linkage). The percolation of edge-sharing units (equivalent to chains of "2" cations) results in an additional ordering of the cation sublattice beyond that imposed by a simple corner-sharing polyhedral network. The percolated edge-sharing units introduce a short cation-cation length scale (across an edge-sharing anion double bridge) resulting in a region of relatively high cation density.

Figure 4 (lower panel) shows the effect of the additional cation-cation length scales on the real space concentration-concentration Bhatia-Thornton functions, $g_{CC}(r)$. The $GeSe_2$ system shows a significant feature at $r/r_{+-} \sim 1.33$ attributable to the existence of a significant number of the percolating edge-sharing units. The presence of the percolating edge-sharing units, therefore, creates fluctuations in the cation subdensity on both short and intermediate length scales. The pseudo-one-dimensional nature of these units leads to fluctuations in the cation charge density over the intermediate length scale and hence causes the FSDP in $S_{CC}(k)$. For $ZnCl_2$, the chain percolation is strictly limited and so these additional length scales are only transient.

In this paper the difference in the intermediate-range order observed in two specific systems ($ZnCl_2$ and $GeSe_2$) has been investigated. The variations in the IRO have been attributed to the difference in the number of edge-sharing tetrahedral units present in the two systems. For $GeSe_2$, these edge-sharing polyhedral units are found to percolate into persistent charge-neutral (one-dimensional) chain structures which act to break up the (three-dimensional) corner-sharing network (predominant in $ZnCl_2$). These chains act to introduce an additional intermediate-ranged length scale leading to an excess intensity in $S_{MM}(k_{FSDP})$ which is not counterbalanced by the corresponding $S_{MX}(k)$ function and hence leads to the FSDP in $S_{CC}(k)$.

M.W. thanks Dr. Philip Salmon (Department of Physics, University of Bath) and Dr. Carlo Massobrio (Institut de Physique et de Chimie des Matériaux de Strasbourg) for useful discussions. The work was supported by EPSRC, Grant No. GR/S06233/01.

[1] S. R. Elliott, Nature (London) **354**, 445 (1991).
[2] P. S. Salmon, Proc. R. Soc. London, Ser. A **445**, 351 (1994).
[3] P. H. Gaskell and D. J. Wallis, Phys. Rev. Lett. **76**, 66 (1996).
[4] S. R. Elliott, J. Non-Cryst. Solids **182**, 40 (1995).
[5] M. Wilson and P. A. Madden, Phys. Rev. Lett. **72**, 3033 (1994); **80**, 532 (1998).
[6] M. Wilson and P. A. Madden, J. Phys.: Condens. Matter **11**, A237 (1999).
[7] W. Götze and L. Sjogren, Rep. Prog. Phys. **55**, 241 (1992).
[8] S. Biggin and J. E. Enderby, J. Phys. C **14**, 3129 (1981).
[9] J. A. E. Desa, A. C. Wright, A. C. Wong, and R. N. Sinclair, J. Non-Cryst. Solids **51**, 57 (1982).
[10] I. Petri, P. S. Salmon, and H. E. Fischer, Phys. Rev. Lett. **84**, 2413 (2000); I. T. Penfold and P. S. Salmon, *ibid.* **67**, 97 (1991); P. S. Salmon and I. Petri, J. Phys.: Condens. Matter **15**, S1509 (2003); I. Petri, P. S. Salmon, and W. S. Howells, *ibid.* **11**, 10219 (1999).
[11] P. S. Salmon, R. A. Martin, P. E. Mason, and G. J. Cuello, Nature (London) **435**, 75 (2005).
[12] J. Neuefeind, Phys. Chem. Chem. Phys. **3**, 3987 (2001).
[13] D. A. Allen, R. A. Howe, N. D. Wood, and W. S. Howells, J. Chem. Phys. **94**, 5071 (1991).
[14] W. A. Crichton, M. Mezouar, T. Grande, S. Stølen, and A. Grzechnik, Nature (London) **414**, 622 (2001).
[15] C. H. Polsky, L. M. Martinez, K. Leinenweber, M. A. VerHelst, C. A. Angell, and G. H. Wolf, Phys. Rev. B **61**, 5934 (2000).
[16] C. Massobrio, F. H. M van Roon, A. Pasquarello, and S. W. De Leeuw, J. Phys.: Condens. Matter **12**, L697 (2000); C. Massobrio, M. Celino, and A. Pasquarello, Phys. Rev. B **70**, 174202 (2004); C. Massobrio, A. Pasquarello, and R. Car, Phys. Rev. Lett. **80**, 2342 (1998); C. Massobrio, A. Pasquarello, and R. Car, Phys. Rev. B **64**, 144205 (2001); C. Massobrio and A. Pasquarello, J. Chem. Phys. **114**, 7976 (2001); C. Massobrio and A. Pasquarello, Phys. Rev. B **68**, 020201 (2003).
[17] M. Cobb, D. A. Drabold, and R. L. Cappelletti, Phys. Rev. B **54**, 12162 (1996); M. Cobb and D. A. Drabold, *ibid.* **56**, 3054 (1997); M. Durandurdu and D. A. Drabold, *ibid.* **65**, 104208 (2002); P. Biswas, D. N. Tafen, and D. A. Drabold, *ibid.* **71**, 054204 (2005).
[18] A. B. Bhatia and D. E. Thornton, Phys. Rev. B **2**, 3004 (1970).
[19] P. S. Salmon, *Proc: Math. and Phys. Sci.* **437**, 591 (1992).
[20] P. Vashishta, R. K. Kalia, G. A. Antonio, and I. Ebbsjö, Phys. Rev. Lett. **62**, 1651 (1989); H. Iyetomi, P. Vashishta, and R. K. Kalia, Phys. Rev. B **43**, 1726 (1991).
[21] P. A. Madden and M. Wilson, Chem. Soc. Rev. **25**, 339 (1996).
[22] C. Domene, P. W. Fowler, P. A. Madden, and M. Wilson, Mol. Phys. **100**, 3847 (2002).
[23] N. C. Pyper, *Advances in Solid-State Chemistry* (JAI, London, 1991), Vol. 2, p. 223.
[24] M. Wilson and P. A. Madden, Mol. Phys. **92**, 197 (1997).
[25] The partial structure factors are calculated from $S_{\alpha\beta}(k) = \langle A^*_\alpha(k) \cdot A_\beta(k) \rangle$, where $A_\alpha(k) = 1/\sqrt{N_\alpha} \Sigma_i e^{i\mathbf{k}.\mathbf{r}_i}$ are the Fourier components.
[26] The cation-cation and cation-anion structure factors can be reconstructed using

$$S_{MM}(k) = c_0^2(S^{00}_{MM} - 1) + c_1^2(S^{11}_{MM} - 1) + c_2^2(S^{22}_{MM} - 1) + 2c_0c_1S^{01}_{MM} + 2c_0c_2S^{02}_{MM} + 2c_1c_2S^{12}_{MM},$$

$$S_{MX}(k) = c_0S^{0X}_{MX} + c_1S^{1X}_{MX} + c_2S^{2X}_{MX},$$

where c_a is the fraction of cation sites colored as a.